Ferroelectric system dynamics simulated by a second-order Landau model

Michael S. Richman, Paul Rulis, and Anthony N. Caruso

Citation: Journal of Applied Physics **122**, 094101 (2017);
View online: https://doi.org/10.1063/1.5000139
View Table of Contents: http://aip.scitation.org/toc/jap/122/9
Published by the American Institute of Physics

Articles you may be interested in

Ferroelectric, pyroelectric, and piezoelectric properties of a photovoltaic perovskite oxide
Applied Physics Letters **110**, 063903 (2017); 10.1063/1.4974735

Ferroelectric or non-ferroelectric: Why so many materials exhibit "ferroelectricity" on the nanoscale
Applied Physics Reviews **4**, 021302 (2017); 10.1063/1.4979015

Static negative capacitance of a ferroelectric nano-domain nucleus
Applied Physics Letters **111**, 152902 (2017); 10.1063/1.4989391

Periodic arrays of flux-closure domains in ferroelectric thin films with oxide electrodes
Applied Physics Letters **111**, 052901 (2017); 10.1063/1.4996232

Measurement of surface acoustic wave resonances in ferroelectric domains by microwave microscopy
Journal of Applied Physics **122**, 074101 (2017); 10.1063/1.4997474

Coexistence of domain relaxation with ferroelectric phase transitions in $BaTiO_3$
Journal of Applied Physics **121**, 184101 (2017); 10.1063/1.4983073

Ferroelectric system dynamics simulated by a second-order Landau model

Michael S. Richman, Paul Rulis, and Anthony N. Caruso[a)]
Department of Physics and Astronomy, University of Missouri-Kansas City, Kansas City, Missouri 64110, USA

(Received 22 May 2017; accepted 13 August 2017; published online 7 September 2017)

By using a second-order time-dependent Ginzburg–Landau model, we simulate the dynamic polarization hysteresis behavior of a ferroelectric system subjected to a sinusoidal electric field. We examine polarization hysteresis loop structure as a function of both field amplitude and field frequency. The relationship between the latter and hysteresis loop area, i.e., hysteresis dispersion, is calculated. Departing from previous work that established that the considered model produces experimentally expected hysteresis dispersion in the low-frequency regime, we demonstrate that (i) this model also produces experimentally expected hysteresis dispersion in the high-frequency regime; (ii) this dispersion implies, in agreement with experimental observations, that system relaxation is characterized by an effective characteristic time which is inversely proportional to field amplitude when the latter is sufficiently high; and (iii) the considered model predicts a symmetry-breaking transition that depends on both field frequency and field amplitude. *Published by AIP Publishing*. [http://dx.doi.org/10.1063/1.5000139]

I. INTRODUCTION

Understanding the electronic response of dielectric materials to radio-frequency electromagnetic fields is an outstanding goal in the solid-state theory.[1] The root of the problem is that electronic phenomena cover such wide ranges of time and length scales that no theory has yet been developed which has practical applicability to all scales in a completely general sense. Therefore, there is significant interest in developing theory that is at least applicable to specific subsets of these scales. The inherent challenge is that there can be many orders-of-magnitude in difference between the timescales over which electric field induced macroscopic property changes occur (e.g., 10^{-9} s for microwaves) and the timescales over which detailed electronic structures may shift and oscillate (i.e., 10^{-16} s). This can be prohibitive for current methods of direct simulation when systems are sufficiently large.[2–7] For example, using first-principles quantum mechanics models to merely determine the atomic and electronic structures of ferroelectric materials, without even considering dynamical properties, is difficult because computational speed is limited and the required algorithms scale poorly as the system size increases.[4] Consequently, simulations typically model not more than several hundreds of atoms.[4] This size restriction can preclude adequately capturing the multiscale physics associated with domains.[8] Worsening the situation, some state-of-the-art theory is not suitable for modeling strongly nonlinear behavior,[9,10] and it is precisely this behavior that is of applied relevance sometimes (e.g., see Refs. 11–17).

Because of these challenges, valuable and otherwise unattainable understanding of the dynamic properties of dielectric materials may be provided by phase-field approaches. One such approach that can be applied to study ferroelectric systems, which can exhibit prominent nonlinear relationships between a system's polarization P and an applied electric field E to which it is subjected, is the time-dependent Ginzburg–Landau (TDGL) methodology. However, because the classical TDGL equation is only first order in time, it fails to model inertial effects. Consequently, when considering a system subjected to an applied electric field oscillating with a frequency ω, this equation can produce increasingly inaccurate predications as ω increases.[18–20] A salient example of this behavior is provided by the inability of this equation to produce the resonance peak associated with the dielectric response of a ferroelectric subjected to a high-frequency applied field.[20]

However, by including a kinetic energy term with the Landau free-energy expansion, B. Wang *et al.* established in Ref. 20 a second-order TDGL model that rectifies the aforementioned inertial deficiency. In Ref. 21, Y.-L. Wang *et al.* applied this model to simulate initial polarization curves and P–E hysteresis loops, i.e., the dependences of P on E. They examined hysteresis loop area as a function of field frequency, i.e., hysteresis dispersion, and confirmed that this model produces the experimentally expected result that loop area increases with ω when the latter is sufficiently low.[21] However, Y.-L. Wang *et al.* concluded that this model is implied to be valid only for low-frequency applied fields because their simulations do not confirm the experimental observation that loop area decreases with increasing ω when the latter is sufficiently high [e.g., higher than 100 Hz in the case of a $Pb(Ti_{0.48}Zr_{0.52})O_3$ ferroelectric system[22]].[21] Similar second-order models have been considered in Refs. 18 and 23–41, but these studies do not examine hysteresis dispersion in the high-frequency regime.

In the present work, we apply the second-order TDGL model of Ref. 20 to simulate a ferroelectric system subjected to a sinusoidal electric field. We examine polarization hysteresis loop structure as a function of both field amplitude and field frequency and confirm the low-frequency dispersion result obtained in Ref. 21. However, we also

[a)]Author to whom correspondence should be addressed: carusoan@umkc.edu

demonstrate that (i) the model of Ref. 20 produces experimentally expected hysteresis dispersion in the high-frequency regime; (ii) this dispersion implies, in agreement with experimental observations, that system relaxation is characterized by an effective characteristic time which is inversely proportional to field amplitude when the latter is sufficiently high; and (iii) the considered model predicts a symmetry-breaking transition that depends on both field frequency and field amplitude.

Our work provides more than just advancement in the development and validation of theory. The *P–E* relationships exhibited by ferroelectric systems, as well as their short response times to applied electric fields,[36] make them interesting candidates for the fabrication of filters and switches that provide passive tunable transmission of radio-frequency electromagnetic fields. For example, it has been predicted that the carrier concentration and resulting conductivity of a two-dimensional electron gas (2DEG) can be altered by the electric field due to the interface polarization of a ferroelectric in close proximity to a 2DEG.[42–44] Because the polarization of a ferroelectric is dependent on an electric field applied to it, a ferroelectric paired with a 2DEG may then result in a system exhibiting a field-dependent switching between a non-conducting (transmissive) and a conducting (non-transmissive) state. However, designing such a system to have particular transmission characteristics requires a model that can accurately relate the field-dependent properties of a ferroelectric system to the parameters on which those properties depend. Establishing the validity of such a model and how to implement it are thus important for realizing particular applications. Furthermore, understanding how ferroelectric polarization hysteresis loops depend on frequency is relevant to a new generation of modulators and rectifiers,[42] as well as data storage devices.[45] Additional information pertaining to the technological benefit of studying the dynamic polarization hysteresis properties of ferroelectric systems is provided by Refs. 21, 42, 45–48, and references therein.

The rest of this article is organized as follows. In Sec. II, we discuss the model, parameters, and numerical method we use. In Sec. III, we discuss results concerning the parameter dependence of polarization hysteresis loop structures and propose an explanation for why a previous study failed to obtain certain of the results that we present. In Sec. IV, we extend the analysis of the preceding section by elaborating on hysteresis dispersion. In Sec. V, we determine and discuss the field-dependent system relaxation times that we obtain from the dispersion curves. In Sec. VI, we consider the symmetry-breaking transition that depends on both field frequency and field amplitude. Finally, in Sec. VII, we summarize our results, discuss information pertaining to model parameters, and point out some previously unmentioned limitations of the considered model.

II. MODEL, PARAMETERS, AND NUMERICAL METHOD

In what follows, we discuss a model of a ferroelectric system where the ferroelectric is taken to be perfectly insulating. For a broader discussion of such systems, though, we refer the reader to Refs. 8 and 49–55. Proceeding as in Ref. 20, we consider a system in a three-dimensional Cartesian coordinate system with dimensions $x \times y \times z = L_x \times L_y \times h$. The polarization P is taken to be directed along the z axis. We examine free-energy contributions from: (i) the Landau free-energy expansion expressed to only sixth order (i.e., terms higher than sixth order are truncated); (ii) the Ginzburg terms; (iii) the depolarization field $\vec{E}_d = (E_x, E_y, E_d)$; (iv) an applied electric field $\vec{E} = (0, 0, E)$; (v) epitaxial stresses $\sigma_{xx} = \sigma_{yy} = \sigma_r$; and (vi) free surfaces. The total system free energy is then provided by

$$\begin{aligned} F = &\iiint_V \left\{ \frac{A}{2}P^2 + \frac{B}{4}P^4 + \frac{C}{6}P^6 + \frac{D_{11}}{2}\left(\frac{\partial P}{\partial z}\right)^2 \right. \\ &\left. + \frac{D_{44}}{2}\left[\left(\frac{\partial P}{\partial x}\right)^2 + \left(\frac{\partial P}{\partial y}\right)^2\right] - \frac{1}{2}E_d P - EP - 2\sigma_r \varepsilon_0 \right\} dv \\ &+ \iint_{S_1} \frac{D_{11}\delta_3^{-1}}{2} P^2 dxdy + \iint_{S_2} \frac{D_{44}\delta_1^{-1}}{2} P^2 dydz \\ &+ \iint_{S_3} \frac{D_{44}\delta_1^{-1}}{2} P^2 dxdz, \end{aligned} \tag{1}$$

where A, B, C, D_{11}, and D_{44} are the bulk material expansion coefficients, S_1, S_2, and S_3 represent the six surface planes, δ_1 and δ_3 are the extrapolation lengths that measure the strengths of the surface effects, and ε_0 is a stress-free strain due to polarization and is given by $\varepsilon_0 = \varepsilon_{xx}^T = \varepsilon_{yy}^T = QP^2$, where Q is an electrostrictive coefficient. D_{11} and D_{44} represent domain-wall energy densities that characterize the energy from dipole–dipole interactions resulting from spatially inhomogeneous polarization.[56] Further elaboration pertaining to Eq. (1) is provided by Refs. 18, 20, 23, 28, 52, and 56–69.

Proceeding with the derivation provided in Ref. 20 where polarization is postulated to have inertia, a kinetic energy term then contributes to the total system energy. This term is given by

$$T = \frac{1}{2}\rho\left(\frac{\partial P}{\partial t}\right)^2, \tag{2}$$

where t denotes time and ρ is the material-dependent effective mass density. The latter is determined by the relation of the mass density of dipoles to the charge density of dipoles.[23]

We mention that although it is not explicitly stated in the reference which established the model that we consider, this model does not account for ferroelectric strain that exhibits relaxation effects or inertial effects. That is, ferroelectric strain at a given time is modeled to depend only on the system polarization at that time. Studies indicate that such behavior can be assumed for many ferroelectric materials when the applied field varies sufficiently slowly.[32,58,70] However, phase-field models exist in the literature that may aid in the construction of a simulation which can capture the relaxation effects and inertial effects that result from polarization-induced strain.[31–33,70–72]

Proceeding with the derivation in Ref. 20, the Lagrange function for the system is then provided by

$$L = \iiint_V T dv - F, \tag{3}$$

and the evolution from time t_1 to t_2 depends on the "*action*" integral given by

$$I = \int_{t_1}^{t_2} L dt. \tag{4}$$

By using a process similar to that used to derive the classical TDGL equation (see, e.g., Refs. 18, 23–25, 32, and 73–75 for insight pertaining to this), one can then obtain the polarization evolution equation given by

$$K\frac{\partial P}{\partial t} = \frac{\delta I}{\delta P} = -\rho\frac{\partial^2 P}{\partial t^2} - AP + 4Q\sigma_r P + E_d + E - BP^3 - CP^5 + D_{11}\frac{\partial^2 P}{\partial z^2} + D_{44}\left(\frac{\partial^2 P}{\partial x^2} + \frac{\partial^2 P}{\partial y^2}\right), \tag{5}$$

where K is a kinetic coefficient related to domain mobility. Information on evaluation of the functional derivative is provided by Ref. 76. We note that $\delta I/\delta P$ can be considered to represent a thermodynamic driving force for the spatial and temporal evolution of the system. As indicated by Ref. 77, this means Eq. (5) is of the form "velocity proportional to force," and this equation describes a viscous-type mechanism where K measures the ability of the system to resist the action of this force. Furthermore, Ref. 21 indicates that $\partial P/\partial t$ is proportional to the material's viscous force, which acts in a direction opposite to that of P. This means that a higher thermodynamic driving force will result in a more viscous material.

Proceeding with the derivation in Ref. 20, the divergence theorem for the electrostatic depolarization potential Φ then provides

$$\frac{\partial^2\Phi}{\partial x^2} + \frac{\partial^2\Phi}{\partial y^2} + \frac{\partial^2\Phi}{\partial z^2} = \frac{1}{\alpha}\frac{\partial P}{\partial z}, \tag{6}$$

where α is the dielectric constant of the ferroelectric without the effect of spontaneous polarization. Then,

$$E_d = -\frac{\partial\Phi}{\partial z}. \tag{7}$$

Proceeding as in Ref. 21, we (i) set $E = E_0\sin(\omega t)$, where E_0 and ω represent the field amplitude and field frequency, respectively; (ii) consider a two-dimensional system in the x–z plane; and (iii) take this system to have periodic boundary conditions. The latter approximation becomes increasingly accurate as the depolarization field resulting from polarization-induced surface charges disappears. In the case of a ferroelectric material sandwiched between two electrodes, this depolarization field has been modeled to vanish as material thickness h increases.[64,78,79] We mention that in the experimental studies which provide the data that we compare our simulation results to, the ferroelectric materials are sandwiched between electrodes. Additional information pertaining to surface characteristics is provided by Refs. 35, 42, 49, 52, 64–68, and 78–112.

Proceeding, we take the initial polarization of the system to be spatially uniform. This provides a monodomain system. Then, because we model neither thermal vibrations (e.g., Refs. 24, 25, 106, and 113–115) nor crystal defects (e.g., Refs. 21 and 116–122), the dynamics of the system is reduced to that of a single differential equation, i.e., a second-order Landau–Khalatnikov equation.[24,25] In the subsequent discussion, we refer to both this equation and the second-order TDGL equation as second-order Landau equations. We note that the second-order Landau–Khalatnikov equation has been referred to as a Landau–Khalatnikov–Tani equation.[24] Furthermore, we mention that this equation results in a polarization evolution expression which is identical in form to the Duffing equation if both $E = E_0\sin(\omega t)$ and the Landau free-energy expansion is expressed to only fourth order.[23,123,124]

The dimensionless variables employed in Ref. 21 are used, i.e., we let

$$\tilde{t} = \sqrt{\frac{|A|}{\rho}}t,$$

$$\tilde{P} = \frac{P}{|P_0|},$$

$$\tilde{E} = \frac{E}{|A||P_0|},$$

and

$$\tilde{\omega} = \omega\sqrt{\frac{\rho}{|A|}}. \tag{8}$$

This provides

$$K\sqrt{\frac{1}{\rho|A|}}\frac{d\tilde{P}}{d\tilde{t}} = -\frac{d^2\tilde{P}}{d\tilde{t}^2} + \left(\frac{4Q\sigma_r}{|A|} - \frac{A}{|A|}\right)\tilde{P} + \tilde{E}_0\sin(\tilde{\omega}\tilde{t}) - \frac{B|P_0|^2}{|A|}\tilde{P}^3 - \frac{C|P_0|^4}{|A|}\tilde{P}^5, \tag{9}$$

where $\tilde{E}_0$ is the normalized amplitude of the applied field.

All of the simulation results displayed in the present work were obtained by using the following parameters from Ref. 21: $A = -4.124\times10^7$ Nm^2/C^2, $B = -2.097\times10^8$ Nm^6/C^4, $C = 3.412\times10^9$ Nm^{10}/C^6, $Q = 0.113$ m^4/C^2, $\sigma_r = 1.3\times10^9$ N/m^2, $P_0 = 0.963$ C/m^2, $\tilde{\omega}_0 = 2\pi/6400$, and $K/\sqrt{\rho/|A|} = 3000$. These selections were made in order to facilitate a comparison of our results with those of Ref. 21. However, we have also performed simulations by using the free-energy coefficients that are provided in Ref. 125 for $BaTiO_3$ and $PbTiO_3$ at temperatures of 100 K and 293.15 K, respectively. These simulations have produced results that are comprehensively qualitatively identical to those which we have obtained by using the coefficients from Ref. 21. Consequently, the qualitative results that we present are expected to be exhibited by

various ferroelectric materials. Polarization and its first-order derivative are initialized to zero.

Equation (9) is solved by using an explicit fourth-order Runge–Kutta method. To meet accuracy requirements at all frequencies considered, the time step is chosen to be $\tilde{T}/10^7$, where $\tilde{T}$ is the normalized period of the applied field. Our numerical method will be discussed again in the last paragraph of Sec. III.

As indicated, we consider a model in which polarization switches only by variation of the modulus of the longitudinal component of polarization that is parallel to the applied field. However, this is not the only mechanism by which a ferroelectric system's polarization may switch in response to a linearly polarized applied field. For example, at crystal defect sites, there may be polarization components that are perpendicular to the axis of such a field.[126] This may result in polarization switching that occurs by polarization vector rotations.[126,127] For perovskite-type ferroelectrics, Ricinschi *et al.* have indicated that such rotations are relatively insignificant when the applied field is sufficiently large.[126] At smaller fields, though, these rotations can be more significant.[126] This occurs for a perovskite-type ferroelectric near to the morphotropic phase boundary, i.e., the boundary between the rhombohedral and tetragonal phases in the concentration–temperature phase diagram.[126] Further discussion pertaining to polarization switching mechanisms is provided in the second paragraph of Sec. V, and we elaborate on defects and other factors that may induce polarization rotation in the last paragraph of Sec. VII.

Before presenting our simulation results in Secs. III–VI, we provide a few comments regarding the model itself. We note that in the case of monodomain systems characterized by Landau-type potentials, there is conflict in the literature regarding whether or not chaotic behavior will be displayed for any combination of E_0 and ω.[23,24,128] We are aware of only one study where a second-order Landau equation is used to study the dynamics resulting from potentials of this type, though, and this work does indicate the onset of chaos when field amplitudes are sufficiently high.[23] We do not attempt to confirm this result. We also mention that in the case of monodomain systems characterized by Landau-type potentials, there is disagreement among previous studies about whether or not polarization oscillations of a frequency identical to that of the applied field will eventually be exhibited for any combination of E_0 and ω.[24,25,128] Our results that address this issue are discussed in Sec. III. We also note that although our simulations are suitable for modeling the behavior of a single crystal, experimental observations indicate that a single-crystal treatment can adequately capture certain characteristics of a polycrystal.[129] Nevertheless, because the characteristics of polycrystals can be distinct from those of single crystals,[130] the reader is referred to Refs. 72 and 73 for information pertaining to phase-field simulations of polycrystals.

III. PARAMETER DEPENDENCE OF HYSTERESIS LOOP STRUCTURES

By using our stated initial conditions, the number of periods of the applied field required for a system to exhibit steady-state behavior increases with ω and decreases as E_0 grows. However, we henceforth consider only steady-state behavior. Under this circumstance, for all field parameters considered, the polarization appears to be periodic in time, though not necessarily sinusoidal. Moreover, P oscillates with the same frequency as that of E, i.e., the P–E curves form closed loops. The structures of these loops depend on the phase shift of the polarization with respect to the applied field. This shift, which will be elaborated on later, is due to the relaxation delay of the system. Hysteresis loops for $\tilde{E}_0 = 100$ and frequencies ranging from $\tilde{\omega} = \tilde{\omega}_0$ to $\tilde{\omega} = 1000\tilde{\omega}_0$ are displayed in Fig. 1. Some corresponding plots of the temporal evolution of both $\tilde{E}$ and $\tilde{P}$ are exhibited in Fig. 2. In the following analysis, we employ the terminology used by Rao *et al.* in their study of magnetic hysteresis in Ref. 131. Figures 1(a)–1(f) indicate that as field frequency increases, loop saturation disappears and the loop shape morphs from being spindle like to being ellipse like. Evident from Figs. 1(d)–1(f) is that once ellipse-like loops appear, the semi-major axis of each loop decreases its angle of inclination with respect to the E axis as the frequency increases.

In what follows, we define the coercive field as the field magnitude at which $P = 0$ when hysteresis loops are not shifted towards the upper half of the P–E plane. To provide physical insight into the parameter dependence of hysteresis loop structures, we emphasize the view advocated by Su *et al.* in their study of nanocrystalline ferroelectric polycrystals in Ref. 73. That is, we consider the frequency dependence of hysteresis loops to result from a competition between the speed associated with the polarization evolution and the speed associated with the applied field. Recalling then that (i) as discussed in Sec. II, our considered polarization evolution model is of the form "velocity proportional to force" and it thus describes a viscous-type mechanism where $\partial P/\partial t$ is proportional to the viscous force; and (ii) increased speed of the polarization evolution is associated with a higher field frequency consistent with the latter being identical to the polarization frequency in the steady state, it becomes evident that the system can become more viscous as ω increases. This means that (i) as ω grows, the polarization should increasingly lag behind the applied field up to some threshold field frequency; and (ii) prior to exceeding this frequency, the coercive field should increase with ω. The former and latter theoretical expectations are confirmed in Figs. 2(a)–2(c) and 1(a)–1(e), respectively. The growth of the coercive field with increasing field frequency can provide a $\tilde{P}$–$\tilde{E}$ loop area $\langle \tilde{A} \rangle$ $(= \oint \tilde{P} d\tilde{E})$ that grows with ω. Such behavior is exhibited in Figs. 1(a)–1(d). Our result that both the coercive field and $\langle \tilde{A} \rangle$ increase with ω when the latter is sufficiently low is in accordance with (i) experimental observations of $Pb(Ti_{0.8}Zr_{0.2})O_3$,[45] $Pb(Ti_{0.48}Zr_{0.52})O_3$,[22,47,132–134] $SrBi_2Ta_2O_9$,[134,135] and Nd-substituted $Bi_4Ti_3O_{12}$ systems;[136] (ii) the results of Ref. 21; and (iii) the predictions of the quasi-static analytical approximation performed by A. Starkov and I. Starkov.[112]

Such increases are not expected for all frequencies, though. For sufficiently high frequencies, the range of polarization values reached by the system is expected to decrease as ω grows. This happens as frequency increases because the

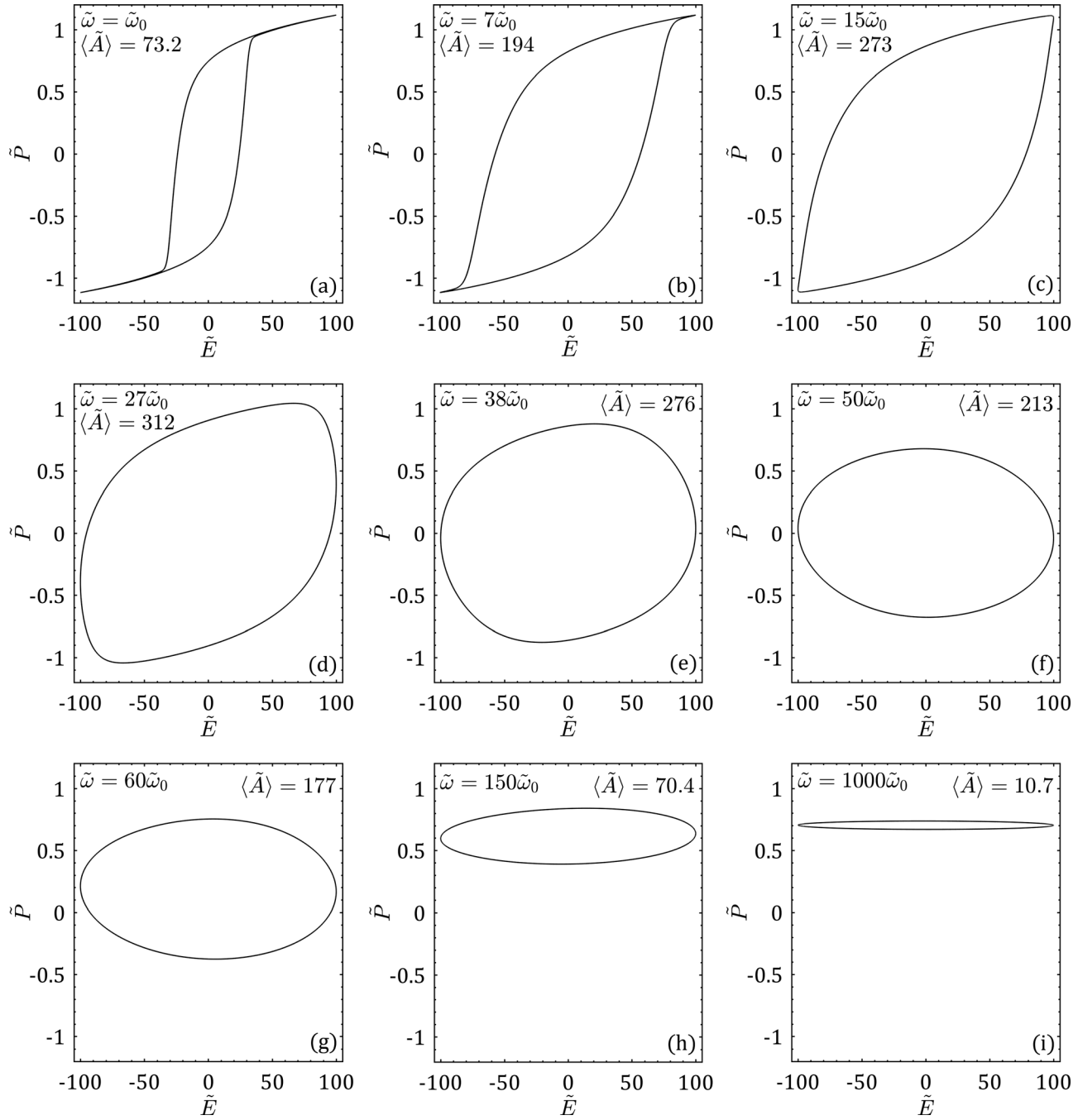

FIG. 1. Steady-state hysteresis loops for $\tilde{E}_0 = 100$ and the field frequencies indicated. The area $\langle \tilde{A} \rangle$ of each loop is displayed.

applied field's characteristic time, which varies inversely with ω, becomes smaller relative to the system's effective relaxation time τ_r. This means that (i) as frequency grows, P–E loop saturation disappears; and (ii) above a critical ω, $\langle \tilde{A} \rangle$ decreases with increasing field frequency. Such behavior is evidenced in Figs. 1(d)–1(f). Another feature pertaining to the two characteristic times, i.e., τ_r and ω^{-1}, is that at sufficiently high frequencies the polarization vector, which initially points in the same direction as the applied field, cannot respond fast enough to undergo a 180° reversal before the applied field returns to pointing in the same direction as this vector. When this occurs, the loop should be shifted upwards in the P–E plane. This expectation is confirmed in Figs. 1(g)–1(i) and 2(d). The initial positive values of E provided by $E = E_0 \sin(\omega t)$ account for the bias towards the upper half of the P–E plane indicated in these figures. We elaborate on this asymmetry in Sec. VI. Our result of a decreasing hysteresis loop area with increasing ω when frequencies are sufficiently high is expected from experimental observations of $Pb(Ti_{0.48}Zr_{0.52})O_3$,[22,47,132–134] $SrBi_2Ta_2O_9$,[134,135] and Nd-substituted $Bi_4Ti_3O_{12}$ systems.[136] We have thus validated the considered model in the high-frequency regime.

We note that it has been pointed out in Ref. 21 that the term $\tilde{\omega}K/\sqrt{\rho}$ determines the P–E relationship if all other model parameters are constant. We have confirmed this result. Recalling that $\tilde{\omega} = \omega\sqrt{\rho/|A|}$ and noting that the normalized applied field is independent of ρ, we arrive at the result emphasized in Ref. 21 that the term $\omega K/\rho$ determines

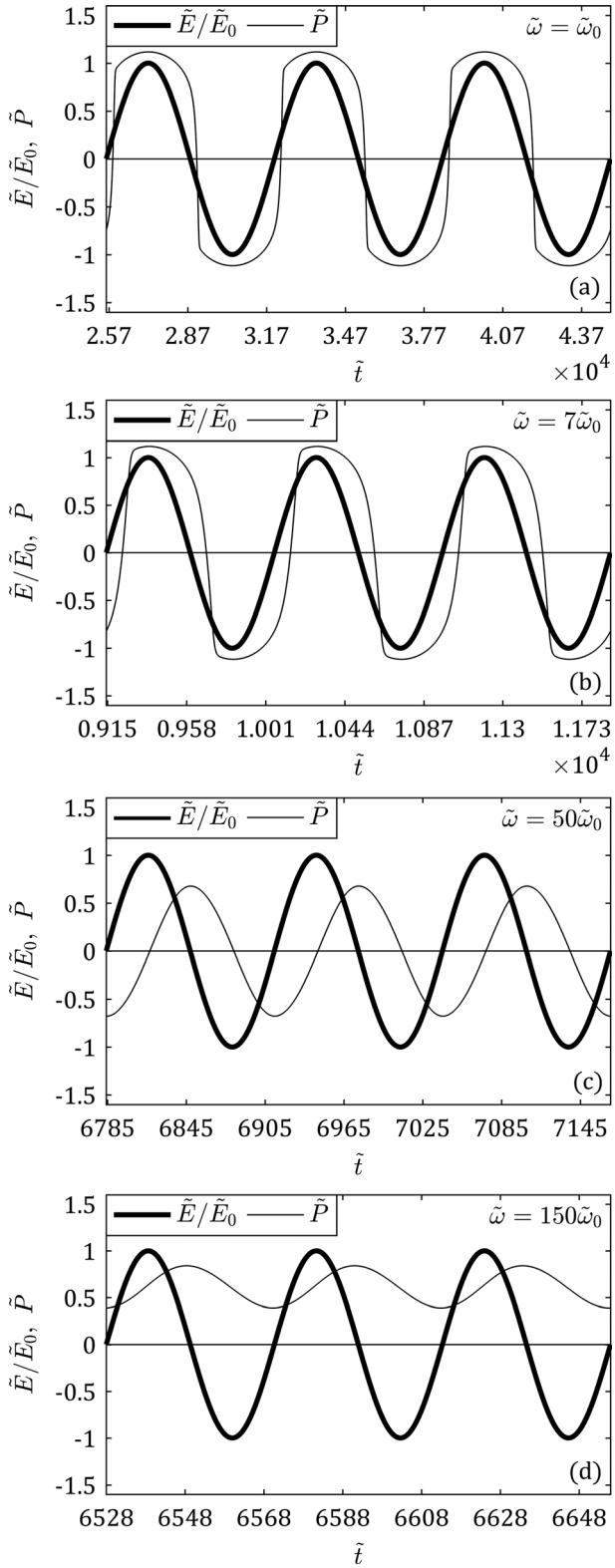

FIG. 2. Temporal evolution of both the applied field and the system polarization once a steady-state condition was reached for $\tilde{E}_0 = 100$ and the field frequencies indicated. The horizontal lines serve as guides to the eye. They do not represent polarization values.

the *P–E* relationship if all other parameters are constant. Similar behavior is indicated in Refs. 73, 137, and 138. We also mention that because we have considered a system with spatially homogeneous polarization, domain-wall energy does not contribute to this system. However, this energy is known to influence the *P–E* relationship when polarization is spatially inhomogeneous. In this case, as the domain-wall energy densities D_{11} and D_{44} of Eq. (1) increase, they can have the effect of constricting polarization hysteresis loops.[80]

Although the dependence of hysteresis loops on field amplitude for a fixed field frequency has been discussed in Ref. 21, for completeness we briefly elaborate on this topic. Hysteresis loops for $\tilde{\omega} = \tilde{\omega}_0$ and amplitudes ranging from $\tilde{E}_0 = 100$ to $\tilde{E}_0 = 350$ are displayed in Fig. 3. In accordance with the results of Ref. 21, as well as experimental observations of $Pb(Ti_{0.48}Zr_{0.52})O_3$,[22,134] $SrBi_2Ta_2O_9$,[134,135] and Nd-substituted $Bi_4Ti_3O_{12}$ systems,[136] we see that both the coercive field and $\langle\tilde{A}\rangle$ increase with $\tilde{E}_0$. Recalling the content of the second paragraph of the present section and noting that Ref. 73 indicates that a higher $\tilde{E}_0$ provides a stronger thermodynamic driving force, these increases in both the coercive field and $\langle\tilde{A}\rangle$ are expected. This is because as the thermodynamic driving force grows, so too can the phase lag of the polarization with respect to the applied field. For additional discussions pertaining to the parameter dependence of hysteresis loop structures, we refer the reader to Refs. 19, 21, 47, 73, 80, 130, 131, 137, and 139.

As mentioned in Sec. I, the experimentally expected trend of a decreasing hysteresis loop area with increasing frequency when the latter is sufficiently high was not obtained when the considered model was applied in Ref. 21. Consequently, it was concluded in this reference that the model is implied to be appropriate only for low frequencies. We now have evidence that counters this point. The aforementioned discrepancy between the results of Ref. 21 and those from experiment may be due to deficient numerical methods and not to an invalid model. Although the computational techniques used to determine the results of Ref. 21 were not clearly specified in this reference, it is suspected that a semi-implicit Fourier-spectral method (e.g., Ref. 140) was employed. While such a technique can decrease computation time, it can also cause inaccuracy.[141] In contrast, we employ an explicit fourth-order Runge–Kutta method.

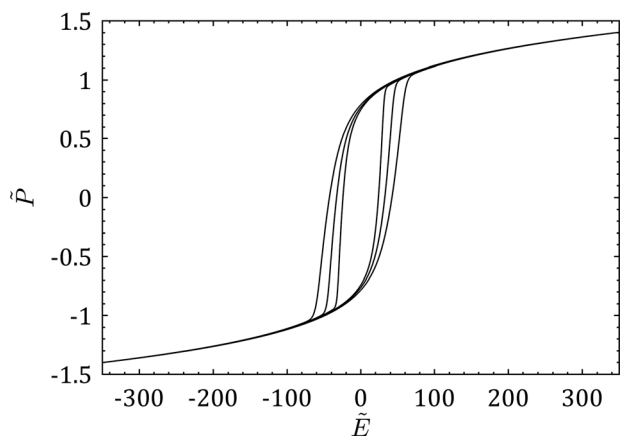

FIG. 3. Steady-state hysteresis loops for $\tilde{E}_0 = 100$, 200, and 350, respectively, from the innermost to the outermost loop. For each loop, $\tilde{\omega} = \tilde{\omega}_0$.

IV. HYSTERESIS DISPERSION

Extending the analysis, we consider $\tilde{P}$–$\tilde{E}$ loop area $\langle\tilde{A}\rangle$ as a function of frequency, i.e., hysteresis dispersion. $\langle\tilde{A}\rangle$ represents the energy dissipated during one cycle of the applied field.[61] Hysteresis dispersion curves for field amplitudes ranging from $\tilde{E}_0 = 100$ to $\tilde{E}_0 = 500$ and from $\tilde{E}_0 = 1500$ to $\tilde{E}_0 = 5500$ are displayed in Figs. 4(a) and 4(b), respectively. For each of these figures, the $\tilde{\omega}/\tilde{\omega}_0$ axis is on a logarithmic scale. We see that each amplitude produces a single-peaked dispersion curve. In accordance with the discussion of Sec. III, the progression towards a smaller $\langle\tilde{A}\rangle$ as $\tilde{\omega} \to 0$ and as $\tilde{\omega} \to \infty$ is consistent with the lower coercive fields present in the former case and the smaller range of polarization values reachable in the latter case. Also evident is that at each frequency, a higher field amplitude produces a larger loop area in agreement with Fig. 3 and the accompanying discussion of it. Additional insight into the behavior indicated in Figs. 4(a) and 4(b) can be obtained by considering that a single-peaked dispersion curve is thought the be a consequence of a competition between the two previously mentioned characteristic times, i.e., τ_r and ω^{-1}.[142,143] When these two times are comparable, a resonance of the domain reversal with respect to the applied field is expected such that $\langle\tilde{A}\rangle$ will be maximized.[143] This means that if τ_r is dependent on $\tilde{E}_0$, so too would be the field frequency at which $\langle\tilde{A}\rangle$ is maximized. This is precisely the behavior indicated in Figs. 4(a) and 4(b). Furthermore, the aforementioned hysteresis dispersion curve shapes and trends are in accordance with experimental observations of $Pb(Ti_{0.48}Zr_{0.52})O_3$,[22,47,132–134] $SrBi_2Ta_2O_9$,[134,135] and Nd-substituted $Bi_4Ti_3O_{12}$ systems.[136] Consequently, the model has been further validated.

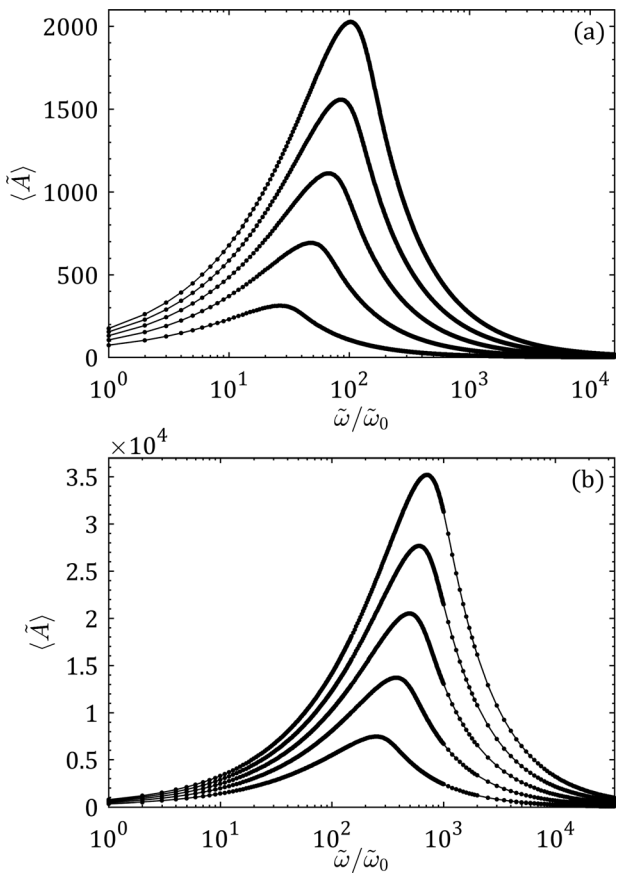

FIG. 4. Hysteresis loop area as a function of frequency for (a) $\tilde{E}_0 = 100$, 200, 300, 400, and 500, respectively, from the lowermost to the uppermost curve and (b) $\tilde{E}_0 = 1500$, 2500, 3500, 4500, and 5500, respectively, from the lowermost to the uppermost curve. For both (a) and (b), the $\tilde{\omega}/\tilde{\omega}_0$ axes are on logarithmic scales and the lines connecting the data points serve as guides to the eye.

V. RELATIONSHIP BETWEEN RELAXATION TIME AND FIELD AMPLITUDE

We can determine the dependence of τ_r on E_0 by using the scaling analysis suggested in Ref. 132. This begins with redefining hysteresis dispersion in terms of $\log(\tilde{\omega}/\tilde{\omega}_0)$ in order to ensure convergence of an arbitrary nth momentum $S_n(\tilde{E}_0) = \int_0^\infty \tilde{\omega}^n \langle\tilde{A}\rangle(\tilde{\omega}, \tilde{E}_0)d\tilde{\omega}$. This provides the scaling parameters

$$\gamma = \log\left(\frac{\tilde{\omega}}{\tilde{\omega}_0}\right),$$

$$S_n(\tilde{E}_0) = \int_{-\infty}^{\infty} \gamma^n \langle\tilde{A}\rangle(\gamma, \tilde{E}_0)d\gamma,$$

$$\gamma_n(\tilde{E}_0) = \frac{S_n(\tilde{E}_0)}{S_0(\tilde{E}_0)},$$

and

$$\tau_1 = 10^{-\gamma_1}, \tag{10}$$

where γ is the modified frequency, γ_n is the nth characteristic frequency, and τ_1 is proportional to τ_r.[134,144,145] Because $\langle\tilde{A}\rangle$ values are small outside the frequency ranges represented in Figs. 4(a) and 4(b), it is adequate to integrate over only these ranges to determine the dependence of τ_1 on $\tilde{E}_0$. This dependence is displayed in Fig. 5 where $\tilde{E}_0^{-1}$ is plotted on the horizontal axis and the solid line, which serves as a guide to the eye, represents an inverse linear relationship between τ_r and $\tilde{E}_0$. This figure implies that when field amplitudes are sufficiently high, an inverse linear correlation exists between τ_1 and $\tilde{E}_0$. When this relationship does not hold, τ_1 is lower

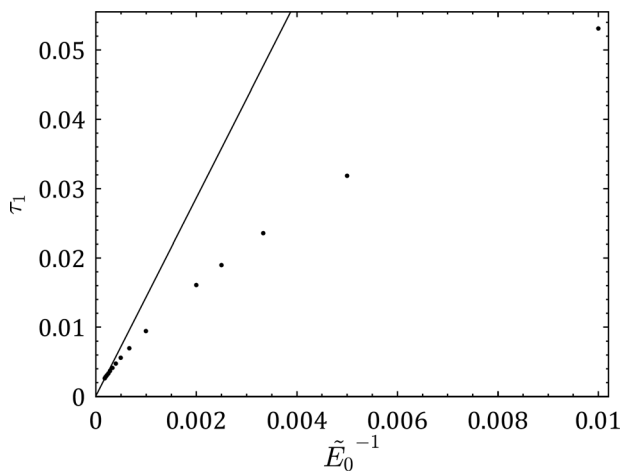

FIG. 5. τ_1 as a function of inverse field amplitude $\tilde{E}_0^{-1}$. The solid line, which serves as a guide to the eye, represents an inverse linear relationship between τ_1 and $\tilde{E}_0$.

than expected from this inverse linear correlation. This scaling behavior obtained for both low- and high-amplitude fields agrees with experimental observations of $Pb(Ti_{0.48}Zr_{0.52})O_3$,[132,134] $SrBi_2Ta_2O_9$,[134,135] and Nd-substituted $Bi_4Ti_3O_{12}$ systems.[136] We have thus further validated the considered model. We note that one study of a model of a ferroelectric system indicates that this model does not produce an inverse linear relationship between τ_1 and E_0 when the latter is extremely large.[143]

We elaborate on the values of τ_1 that we obtained which are lower than expected from the inverse linear correlation that exists between this parameter and $\tilde{E}_0$ when the latter is sufficiently large. For spin systems, it has been suggested that the response speed of domain boundary migration is slower than that of domain rotation.[132] Because the latter mechanism of domain switching may be dominant when field amplitudes are small, it is thought that at small field amplitudes, values of τ_1 may be lower than expected from the inverse linear correlation which exists at larger amplitudes.[132] However, we have obtained such lower values of τ_1 by using a model that captures polarization switching which occurs only by homogeneous variation of the modulus of the longitudinal component of polarization. This means that an alternative explanation for the deviation from an inverse linear correlation exists in the case of the considered model. Additional insight pertaining to the behavior exhibited in Fig. 5 might be provided by Refs. 126, 127, 132, 134, 138, 143, and 145–153.

Establishing a relationship between τ_r and E_0 is not only relevant to the development and validation of theory. If τ_r is in units of seconds and ω is in units of hertz, complete domain reversal will occur when $\tau_r < \omega^{-1}$, i.e., if frequencies are sufficiently low.[134] However, domain reversal cannot fully transpire when $\tau_r > \omega^{-1}$, i.e., if frequencies are sufficiently high.[134] Knowing, then, the relationship between τ_r and E_0 enables a convenient prediction of the field amplitude necessary to produce complete domain reversal at a particular ω. Considering that an interest exists in using ferroelectrics to achieve tunable transmission of radio-frequency electromagnetic fields, and that some of the ways this may occur can depend on complete or incomplete domain reversal, this predictive capability may be of applied relevance.

VI. SYMMETRY-BREAKING TRANSITION

We elaborate on the symmetry-breaking transition that occurs when ω is sufficiently high and E_0 is sufficiently low. Such a transition may also be referred to as a *dynamic phase transition*[128] or a *dynamic transition*.[154] In the steady state, P–E curves appear to form closed loops for all the considered values of both ω and E_0. However, depending on the values of these parameters, one of the two loop types is observed. One type is characterized by a symmetry that is identical to a symmetry of the applied field, i.e., $X(t) = -X(t + T/2)$, where T is the polarization period (and the field period) and X denotes P or E. A system that exhibits this property is considered to undergo a *symmetry-restoring oscillation* (SRO).[155] The other loop type is characterized by a symmetry that is distinct from a symmetry of the applied field, i.e., $X(t) \neq -X(t + T/2)$. A system that displays this behavior is considered to undergo a *symmetry-breaking oscillation* (SBO).[155] Average polarization, which is zero for SRO cycles and nonzero for SBO cycles, serves as an order parameter that distinguishes these two types of oscillations. This metric as a function of field frequency for various field amplitudes is displayed in Fig. 6. We see that for frequencies less than an $\tilde{E}_0$-dependent critical frequency, which is subsequently referred to as $\tilde{\omega}_c$, all examined amplitudes produce SRO cycles. For $\tilde{\omega} > \tilde{\omega}_c$, though, SBO cycles are observed. We have thus demonstrated that a second-order Landau equation produces evidence of a symmetry-breaking transition for a ferroelectric system. The bifurcation curve for this transition is displayed in Fig. 7. It indicates that $\tilde{E}_0$ is nearly proportional to $\tilde{\omega}_c$ over the range of parameters examined. Similar behavior was obtained in Ref. 128 by using theoretical approaches to study a monodomain system characterized by a Landau-type potential, and comparable results were obtained in Ref. 155. However, the models considered in these references are only first order in time. In contrast, we have considered a second-order model. Consequently, Figs. 6 and 7 not only provide the relationship between field frequency and symmetry breaking, but also indicate how the latter depends on both K and ρ. This follows from the discussion in the fourth paragraph of Sec. III where it was mentioned that the term $\omega K/\rho$ determines the P–E relationship if all other model parameters are constant.

We mention that relative to magnetic systems, little attention has been given to the symmetry-breaking transition properties of ferroelectrics,[154] and it is interesting to ask whether or not ferroelectrics typically exhibit a bifurcation curve similar to that of Fig. 7. Insight into this issue is provided by the simulations that we performed by using the aforementioned free-energy coefficients for $BaTiO_3$ and $PbTiO_3$. These simulations indicate that each of these materials undergoes a symmetry-breaking transition where, as in Fig. 7, $\tilde{E}_0$ is nearly proportional to $\tilde{\omega}_c$ over the range of parameters examined for each material. However, such behavior should not be considered to represent a general rule

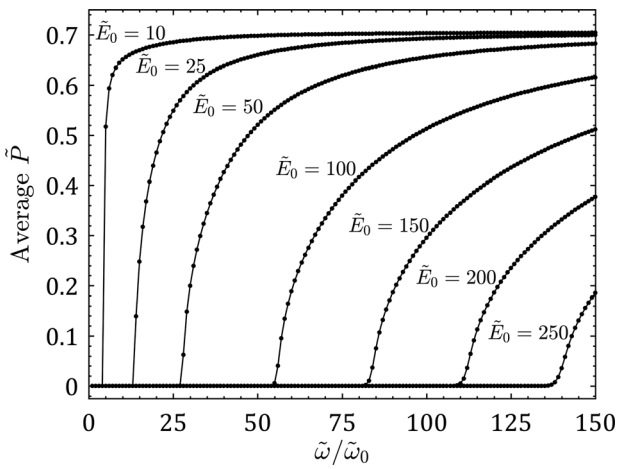

FIG. 6. Average polarization as a function of frequency for the field amplitudes indicated. The lines connecting the data points serve as guides to the eye.

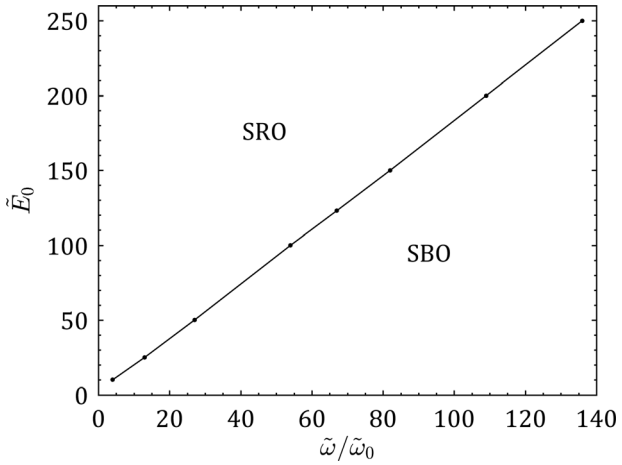

FIG. 7. Bifurcation curve indicating whether a symmetry-restoring oscillation (SRO) or a symmetry-breaking oscillation (SBO) exists for the field parameters indicated. The lines connecting the data points serve as a guide to the eye.

for all physical systems. For example, a study of an anisotropic *XY* spin system that exhibits Ising-type motion has produced a bifurcation curve which, unlike that of Fig. 7, does not exhibit a nearly proportional relationship between field amplitude and the critical frequency above which SBO cycles occur.[156] For additional discussions pertaining to symmetry-breaking transitions, we refer the reader to Refs. 47, 128, 131, and 154–157.

VII. CONCLUSION

By using a second-order TDGL model, we simulated the dynamic polarization hysteresis behavior of a ferroelectric system subjected to a sinusoidal electric field. Polarization hysteresis loop structure as a function of both field amplitude and field frequency were examined. Departing from previous work that established that the considered model produces experimentally expected hysteresis dispersion in the low-frequency regime, we demonstrated that (i) this model also produces experimentally expected hysteresis dispersion in the high-frequency regime; (ii) this dispersion implies, in agreement with experimental observations, that system relaxation is characterized by an effective characteristic time which is inversely proportional to field amplitude when the latter is sufficiently high; and (iii) the considered model predicts a symmetry-breaking transition that depends on both field frequency and field amplitude.

With the considered model now validated and employed to predict the mentioned transition, there is renewed relevance in determining the material-dependent parameters necessary for obtaining increased predicative capabilities with this model. Free-energy coefficients for numerous materials are available, and in some cases, the temperature dependences of these coefficients are indicated.[2,60,69,125,158–168] Furthermore, first-principles calculations can provide such coefficients.[2,60,162–167] Information pertaining to the material-dependent kinetic coefficient K is somewhat scare, though. Regarding this parameter, we mention that Refs. 18, 19, 32, 70–72, 129, and 169 provide experimentally informed phase-field kinetic coefficients for ferroelectric systems. Additionally, temperature-dependent approximations for K are provided in Refs. 169 and 170. In the latter reference, the approximation indicates that K depends on a material-specific polarization relaxation time which itself depends on the strength of the applied electric field. Therefore, for some applications, it may be beneficial to examine the effects of this field dependence of K on polarization evolution. We also note that considering the aforementioned temperature dependences is relevant because of the E_0- and ω-dependent self-heating of a ferroelectric system which results from the cycling of an applied field.[61,171,172] Proceeding with a discussion of parameter determination, we mention that information regarding the material-dependent effective mass density ρ is also rather scant. We note that one attempt to obtain an experimentally informed phase-field inertial term for a ferroelectric system failed to produce a nonzero value for this parameter.[18] However, a nonzero value for ρ has been obtained for $BaTiO_3$.[173–175] Moreover, we mention that ρ is associated with a material's plasma frequency.[24,25] Furthermore, Caputo *et al.* indicate that ρ is proportional to K for a given material.[36] We also note that the incorporation of memory effects into the classical (first-order) TDGL equation by using a decaying exponential memory function characterized by a decay time τ can result in an equation identical in form to the second-order TDGL equation considered in the present work.[176] This means that if a material's polarization decay time is determined, this material's effective mass density can be obtained.

However, ferroelectric materials consist of both an ionic subsystem and a much less massive electronic subsystem,[26] and the response of the former to an applied field can be distinct from that of the latter.[26,62,177,178] Indeed, the difference in subsystem responses can be so pronounced that at optical frequencies the ionic-subsystem polarization can be taken as static in the adiabatic approximation for the electronic-subsystem polarization.[26] Because distinct subsystem responses exist, obtainment of a polarization evolution model that is simultaneously computationally feasible and sufficiently accurate for high frequencies or a large frequency bandwidth may require consideration of an ionic-subsystem phase field coupled to an electronic-subsystem phase field.

Before concluding this article, we mention that although homogeneous polarization switching is exhibited by some ultrathin ferroelectric systems,[179–184] other ferroelectric systems exhibit polarization switching that transpires by a nucleation-and-growth process.[116,185–187] In this process, localized nucleation of reversed domains occurs followed by their growth and possible coalescence. When this happens, coercive fields, which indicate the ease of domain reversal,[188] can be much smaller than those predicted by a model that captures only the homogeneous mechanism of polarization switching.[118] Models that incorporate thermal vibrations,[113,189] surface effects,[80,107,111,122] space charges,[111,190] and dipolar defects[21,118,122,126,137,138] may cause the nucleation-and-growth process and, consequently, increase agreement with experimental observations by decreasing the predicted coercive fields. Such decreases occur because these models can lower the energy required to locally switch polarization.[184] The energy then needed to reverse the

polarization of an entire system can be less than what it would be in the case where reversal occurs homogenously.[184] Of course, as we have discussed, coercive fields also depend on the frequency of the applied field, and we have now validated a model that captures experimentally expected frequency-dependent behavior. A next step is to consider a model that also captures the factors that cause the nucleation-and-growth process. This is left as a topic for future investigation.

ACKNOWLEDGMENTS

The authors would like to thank Ralph Skomski, Peter Dowben, John Mangeri, John Lancaster, and Stephan Young for helpful discussions. This work was supported by the Office of Naval Research under Award No. N00014-16-1-2067.

[1]J. Baker-Jarvis and S. Kim, J. Res. Natl. Inst. Stand. Technol. **117**, 1 (2012).
[2]B. Völker, P. Marton, C. Elsässer, and M. Kamlah, Continuum. Mech. Thermodyn. **23**, 435 (2011).
[3]T. Nishimatsu, U. V. Waghmare, Y. Kawazoe, and D. Vanderbilt, Phys. Rev. B **78**, 104104 (2008).
[4]Y. Zhang, R. Xu, B. Liu, and D. Fang, J. Mech. Phys. Solids **60**, 1383 (2012).
[5]M. Sepliarsky, A. Asthagiri, S. R. Phillpot, M. G. Stachiotti, and R. L. Migoni, Curr. Opin. Solid State Mater. Sci. **9**, 107 (2005).
[6]G. Geneste, J.-M. Kiat, H. Yokota, and Y. Uesu, Phys. Rev. B **83**, 184202 (2011).
[7]G. Geneste, L. Bellaiche, and J.-M. Kiat, Phys. Rev. Lett. **116**, 247601 (2016).
[8]U. V. Waghmare, Acc. Chem. Res. **47**, 3242 (2014).
[9]K. Burke, J. Werschnik, and E. K. U. Gross, J. Chem. Phys. **123**, 062206 (2005).
[10]P. Elliott, F. Furche, and K. Burke, *Reviews in Computational Chemistry* (John Wiley & Sons, Inc., 2008), pp. 91–165.
[11]M. B. Okatan, A. L. Roytburd, J. V. Mantese, and S. P. Alpay, J. Appl. Phys. **105**, 114106 (2009).
[12]Z. Li, Q. Liu, S. Han, T. Iitaka, H. Su, T. Tohyama, H. Jiang, Y. Dong, B. Yang, F. Zhang, Z. Yang, and S. Pan, Phys. Rev. B **93**, 245125 (2016).
[13]M. J. Adams, Solid-State Electron. **30**, 43 (1987).
[14]K. Tilbury and P. Campagnola, Perspect. Med. Chem. **7**, 21 (2015).
[15]W. Nie, Adv. Mater. **5**, 520 (1993).
[16]C. Fuentes-Hernandez, G. Ramos-Ortiz, S.-Y. Tseng, M. P. Gaj, and B. Kippelen, J. Mater. Chem. **19**, 7394 (2009).
[17]C. K. Lin, L. Yang, M. Hayashi, C. Y. Zhu, Y. Fujimura, Y. R. Shen, and S. H. Lin, J. Chin. Chem. Soc. **61**, 77 (2014).
[18]L. X. Wang and M. Willatzen, J. Eng. Mech. **133**, 506 (2007).
[19]L. Wang and M. Willatzen, IEEE Trans. Ultrason. Ferroelectr. Freq. Control **54**, 177 (2007).
[20]B. Wang, H. Fan, and C. H. Woo, J. Appl. Phys. **94**, 3384 (2003).
[21]Y.-L. Wang, X.-Y. Wang, L.-Z. Chu, Z.-C. Deng, X.-C. Ding, W.-H. Liang, P.-C. Zhang, L. Liu, B.-T. Liu, and G.-S. Fu, J. Mater. Sci. **46**, 2695 (2011).
[22]J.-M. Liu, H. P. Li, C. K. Ong, and L. C. Lim, J. Appl. Phys. **86**, 5198 (1999).
[23]A. K. Bandyopadhyay, P. C. Ray, and V. Gopalan, J. Appl. Phys. **100**, 114106 (2006).
[24]S. Sivasubramanian and A. Widom, e-print arXiv:cond-mat/0106549.
[25]S. Sivasubramanian, A. Widom, and Y. N. Srivastava, Ferroelectrics **300**, 43 (2004).
[26]M. D. Glinchuk, E. A. Eliseev, and V. A. Stephanovich, Phys. Solid State **44**, 953 (2002).
[27]M. D. Glinchuk, E. A. Eliseev, V. A. Stephanovich, M. G. Karkut, and R. Farhi, e-print arXiv:cond-mat/0004258.
[28]R. Blinc and B. Žekš, *Soft Modes in Ferroelectrics and Antiferroelectrics* (North-Holland Publishing Co., Amsterdam, 1974).
[29]V. G. Vaks, *Introduction to the Microscopic Theory of Ferroelectrics* (Nauka, Moscow, 1973).
[30]M. D. Glinchuk, E. A. Eliseev, V. A. Stephanovich, M. G. Karkut, R. Farhi, and L. Jastrabik, Integr. Ferroelectr. **38**, 143 (2001).
[31]L. Wang and R. V. N. Melnik, Smart Mater. Struct. **18**, 074011 (2009).
[32]L. Wang, in *ASME 2008 Conference on Smart Material Adaptive Structures Intelligent System*, Ellicott City, Maryland, USA (2008), pp. 189–195.
[33]L. Wang, R. Melnik, and F. Lv, Front. Mech. Eng. **6**, 287 (2011).
[34]D. R. Tilley and B. Žekš, Solid State Commun. **49**, 823 (1984).
[35]M. G. Cottam, D. R. Tilley, and B. Žekš, J. Phys. C: Solid State Phys. **17**, 1793 (1984).
[36]J.-G. Caputo, A. I. Maimistov, E. D. Mishina, E. V. Kazantseva, and V. M. Mukhortov, Phys. Rev. B **82**, 094113 (2010).
[37]J. Osman, Y. Ishibashi, and D. R. Tilley, Jpn. J. Appl. Phys. **37**, 4887 (1998).
[38]R. Murgan, D. R. Tilley, Y. Ishibashi, J. F. Webb, and J. Osman, J. Opt. Soc. Am. B **19**, 2007 (2002).
[39]J. Osman, S.-C. Lim, and D. R. Tilley, J. Korean Phys. Soc. **32**, S446 (1998).
[40]J. F. Webb, Int. J. Mod. Phys. B **17**, 4355 (2003).
[41]J. F. Webb, in *Sixteenth IEEE International Symposium on Applications of Ferroelectrics, 2007. ISAF* (2007), pp. 259–261.
[42]A. I. Kurchak, E. A. Eliseev, S. V. Kalinin, M. V. Strikha, and A. N. Morozovska, e-print arXiv:1703.06500.
[43]A. Rajapitamahuni, J. Hoffman, C. H. Ahn, and X. Hong, Nano Lett. **13**, 4374 (2013).
[44]Y. Wang, M. K. Niranjan, S. S. Jaswal, and E. Y. Tsymbal, Phys. Rev. B **80**, 165130 (2009).
[45]S. M. Yang, J. Y. Jo, T. H. Kim, J.-G. Yoon, T. K. Song, H. N. Lee, Z. Marton, S. Park, Y. Jo, and T. W. Noh, Phys. Rev. B **82**, 174125 (2010).
[46]J.-M. Liu, H. L. Chan, and C. L. Choy, Mater. Lett. **52**, 213 (2002).
[47]J.-M. Liu, Q. Xiao, Z. G. Liu, H. L. W. Chan, and N. B. Ming, Mater. Chem. Phys. **82**, 733 (2003).
[48]T. K. Song, S. Aggarwal, A. S. Prakash, B. Yang, and R. Ramesh, Appl. Phys. Lett. **71**, 2211 (1997).
[49]M. Dawber, K. M. Rabe, and J. F. Scott, Rev. Mod. Phys. **77**, 1083 (2005).
[50]P. Ghosez and J. Junquera, e-print arXiv:cond-mat/0605299.
[51]M. Dawber, P. Chandra, P. B. Littlewood, and J. F. Scott, J. Phys. Condens. Matter **15**, L393 (2003).
[52]P. Chandra and P. B. Littlewood, *Physics of Ferroelectrics: A Modern Perspective* (Springer, Berlin, Heidelberg, 2007), pp. 69–116.
[53]N. Setter, D. Damjanovic, L. Eng, G. Fox, S. Gevorgian, S. Hong, A. Kingon, H. Kohlstedt, N. Y. Park, G. B. Stephenson, I. Stolitchnov, A. K. Taganstev, D. V. Taylor, T. Yamada, and S. Streiffer, J. Appl. Phys. **100**, 051606 (2006).
[54]D. Damjanovic, Rep. Prog. Phys. **61**, 1267 (1998).
[55]F. Yang, G. Hu, B. Xu, W. Wu, C. Yang, and H. Wu, J. Appl. Phys. **112**, 034113 (2012).
[56]S. Li and X. Gao, *Handbook Of Micromechanics Nanomechanics* (Pan Stanford, Singapore, 2013), pp. 73–140.
[57]M. E. Lines and A. M. Glass, *Principles and Applications of Ferroelectrics and Related Materials* (Oxford University Press, New York, 2001).
[58]Y. L. Li, S. Y. Hu, Z. K. Liu, and L. Q. Chen, Appl. Phys. Lett. **78**, 3878 (2001).
[59]C. Wang, *Ferroelectrics* (InTech, 2010), pp. 275–300.
[60]B. Völker, C. M. Landis, and M. Kamlah, Smart Mater. Struct. **21**, 035025 (2012).
[61]R. Smith, *Smart Material Systems: Model Development* (Society for Industrial and Applied Mathematics, 2005), pp. 43–137.
[62]K. Uchino, *Ferroelectric Devices*, 2nd ed. (CRC Press, Boca Raton, FL, 2009).
[63]L.-Q. Chen, J. Am. Ceram. Soc. **91**, 1835 (2008).
[64]Q. Y. Qiu and V. Nagarajan, J. Appl. Phys. **102**, 104113 (2007).
[65]A. M. Bratkovsky and A. P. Levanyuk, J. Comput. Theor. Nanosci. **6**, 465 (2009).
[66]Y. Watanabe, Ferroelectrics **406**, 35 (2010).
[67]Y. Watanabe, J. Phys. Soc. Jpn. **79**, 034713 (2010).
[68]Y. Watanabe, Ferroelectrics **461**, 38 (2014).
[69]B. Wang, *Mechanics of Advanced Functional Materials* (Springer-Verlag, Berlin, Heidelberg, 2013), pp. 321–375.
[70]L. Wang, R. Liu, and R. V. N. Melnik, Sci. China Ser. E: Technol. Sci. **52**, 141 (2009).
[71]L. X. Wang, Y. Chen, and W. L. Zhao, Adv. Mater. Res. **47–50**, 65 (2008).

[72]D. Wang, L. Wang, and R. Melnik, Phys. Lett. A **381**, 344 (2017).
[73]Y. Su, N. Liu, and G. J. Weng, Acta Mater. **87**, 293 (2015).
[74]Y. Su and C. M. Landis, J. Mech. Phys. Solids **55**, 280 (2007).
[75]J.-G. Caputo, E. V. Kazantseva, and A. I. Maimistov, Phys. Rev. B **75**, 014113 (2007).
[76]I. Gyarmati, *Non-Equilibrium Thermodynamics Field Theory Variational Principles* (Springer-Verlag, 1970), pp. 162–167.
[77]G. Bertotti, *Hysteresis in Magnetism for Physicists, Materials Scientists, and Engineers* (Academic Press, San Diego, 1998), pp. 31–72.
[78]A. M. Bratkovsky and A. P. Levanyuk, e-print arXiv:cond-mat/0601484.
[79]R. R. Mehta, B. D. Silverman, and J. T. Jacobs, J. Appl. Phys. **44**, 3379 (1973).
[80]L. Baudry and J. Tournier, J. Appl. Phys. **90**, 1442 (2001).
[81]W. L. Zhong, B. D. Qu, P. L. Zhang, and Y. G. Wang, Phys. Rev. B **50**, 12375 (1994).
[82]Y. Zheng, B. Wang, and C. H. Woo, Phys. Lett. A **368**, 117 (2007).
[83]K. Binder, Ferroelectrics **35**, 99 (1981).
[84]A. Musleh Alrub and L.-H. Ong, J. Appl. Phys. **109**, 084109 (2011).
[85]A. M. Alrub and L.-H. Ong, Eur. Phys. J. B **88**, 9 (2015).
[86]A. M. Musleh, L.-H. Ong, and D. R. Tilley, J. Appl. Phys. **105**, 061602 (2009).
[87]L. Cui, X. Xu, J. Che, Z. He, H. Xue, and T. Lv, J. Mod. Phys. **02**, 1037 (2011).
[88]L. Cui, Q. Xu, Z. Han, X. Xu, J. Che, H. Xue, and T. Lü, Solid State Sci. **16**, 65 (2013).
[89]C. L. Wang and S. R. P. Smith, Solid State Commun. **99**, 559 (1996).
[90]C. L. Wang, L. Zhang, W. L. Zhong, and P. L. Zhang, Phys. Lett. A **254**, 297 (1999).
[91]C. L. Wang, L. Zhang, Y. P. Peng, W. L. Zhong, P. L. Zhang, and Y. X. Wang, Solid State Commun. **109**, 213 (1998).
[92]L.-H. Ong and A. Musleh, Ferroelectrics **380**, 150 (2009).
[93]Z.-D. Zhou, C.-Z. Zhang, and Q. Jiang, Chin. Phys. B **20**, 107701 (2011).
[94]L. Cui, Z. Han, Q. Xu, X. Xu, Y. Gao, J. Che, and T. Lü, Phys. Status Solidi B **250**, 1804 (2013).
[95]L. Cui, H. Cui, C. Wu, G. Yang, Z. He, Y. Wang, and J. Che, Surf. Rev. Lett. **23**, 1650010 (2016).
[96]B. Wang and C. H. Woo, J. Appl. Phys. **97**, 084109 (2005).
[97]R. Kretschmer and K. Binder, Phys. Rev. B **20**, 1065 (1979).
[98]Y. Cao and S. V. Kalinin, Phys. Rev. B **94**, 235444 (2016).
[99]S. V. Kalinin, Y. Kim, D. Fong, and A. Morozovska, e-print arXiv:1612.08266.
[100]D. R. Tilley and B. Zeks, Ferroelectrics **134**, 313 (1992).
[101]D. R. Tilley, *Ferroelectric Ceramics* (Birkhauser, Berlin, 1993), pp. 163–183.
[102]A. M. Bratkovsky and A. P. Levanyuk, Appl. Phys. Lett. **89**, 253108 (2006).
[103]M. Stengel, D. Vanderbilt, and N. A. Spaldin, Nat. Mater. **8**, 392 (2009).
[104]T. M. Shaw, S. Trolier-McKinstry, and P. C. McIntyre, Annu. Rev. Mater. Sci. **30**, 263 (2000).
[105]J. Junquera and P. Ghosez, J. Comput. Theor. Nanosci. **5**, 2071 (2008).
[106]A. Artemev, Philos. Mag. **90**, 89 (2010).
[107]Y. Xia and J. Wang, Smart Mater. Struct. **21**, 094019 (2012).
[108]L. Cui, Z. Han, Z. Qiu, S. Hao, X. Li, J. Che, Q. Xu, and T. Lü, Chin. J. Phys. **52**, 1091 (2014).
[109]A. K. Tagantsev, C. Pawlaczyk, K. Brooks, M. Landivar, E. Colla, and N. Setter, Integr. Ferroelectr. **6**, 309 (1995).
[110]A. K. Tagantsev and G. Gerra, J. Appl. Phys. **100**, 051607 (2006).
[111]V. C. Lo, J. Appl. Phys. **94**, 3353 (2003).
[112]A. Starkov and I. Starkov, Ferroelectrics **461**, 50 (2014).
[113]A. Leschhorn and H. Kliem, J. Appl. Phys. **121**, 014103 (2017).
[114]O. T. Valls and G. F. Mazenko, Phys. Rev. B **42**, 6614 (1990).
[115]I. Aulika and E. Klotins, J. Optoelectron. Adv. Mater. **5**, 747 (2003).
[116]D. Ricinschi and M. Okuyama, Ferroelectrics **349**, 111 (2007).
[117]D. Ricinschi, Y. Ishibashi, M. Iwata, L. Mitoseriu, and M. Okuyama, in *2002 Proceedings of the 13th IEEE Int. Symposium on Applied Ferroelectrics 2002 ISAF* (IEEE, 2002), pp. 79–82.
[118]R. Ahluwalia and W. Cao, Phys. Rev. B **63**, 012103 (2000).
[119]R. Ahluwalia and W. Cao, Ferroelectrics **251**, 191 (2001).
[120]S. Semenovskaya and A. G. Khachaturyan, J. Appl. Phys. **83**, 5125 (1998).
[121]J.-M. Liu, X. Wang, H. L. W. Chan, and C. L. Choy, Phys. Rev. B **69**, 094114 (2004).
[122]D. Ricinschi and M. Okuyama, J. Eur. Ceram. Soc. **25**, 2357 (2005).
[123]S. D. Machado, R. W. Rollins, D. T. Jacobs, and J. L. Hartman, Am. J. Phys. **58**, 321 (1990).
[124]D. L. Mills, *Nonlinear Optics Basic Concepts*, 1st ed. (Springer, 1991), pp. 155–166.
[125]L. Q. Chen, *Physics of Ferroelectrics: A Modern Perspective* (Springer, 2007), pp. 363–371.
[126]D. Ricinschi, Y. Ishibashi, M. Iwata, and M. Okuyama, Jpn. J. Appl. Phys. **40**, 4990 (2001).
[127]M. Iwata, H. Orihara, and Y. Ishibashi, Jpn. J. Appl. Phys. **40**, 708 (2001).
[128]H. Fujisaka, H. Tutu, and P. A. Rikvold, Phys. Rev. E **63**, 036109 (2001).
[129]B. X. Xu, D. Schrade, R. Müller, D. Gross, T. Granzow, and J. Rödel, ZAMM - J. Appl. Math. Mech. Z. Für Angew. Math. Mech. **90**, 623 (2010).
[130]L. Jin, F. Li, and S. Zhang, J. Am. Ceram. Soc. **97**, 1 (2014).
[131]M. Rao, H. R. Krishnamurthy, and R. Pandit, Phys. Rev. B **42**, 856 (1990).
[132]J.-M. Liu, H. L. W. Chan, C. L. Choy, Y. Y. Zhu, S. N. Zhu, Z. G. Liu, and N. B. Ming, Appl. Phys. Lett. **79**, 236 (2001).
[133]J.-M. Liu, Q. C. Li, W. M. Wang, X. Y. Chen, G. H. Cao, X. H. Liu, and Z. G. Liu, J. Phys. Condens. Matter **13**, L153 (2001).
[134]J.-M. Liu, B. Pan, K. F. Wang, and H. Yu, Ceram. Int. **30**, 1471 (2004).
[135]B. Pan, H. Yu, D. Wu, X. H. Zhou, and J.-M. Liu, Appl. Phys. Lett. **83**, 1406 (2003).
[136]J. M. Liu, B. Pan, H. Yu, and S. T. Zhang, J. Phys. Condens. Matter **16**, 1189 (2004).
[137]A. Picinin, M. H. Lente, J. A. Eiras, and J. P. Rino, Phys. Rev. B **69**, 064117 (2004).
[138]J. P. Rino, A. Picinin, M. H. Lente, and J. A. Eiras, Ferroelectrics **300**, 173 (2004).
[139]M. H. Lente, A. Picinin, J. P. Rino, and J. A. Eiras, J. Appl. Phys. **95**, 2646 (2004).
[140]L. Q. Chen and J. Shen, Comput. Phys. Commun. **108**, 147 (1998).
[141]H. G. Lee and J.-Y. Lee, Comput. Math. Appl. **68**, 174 (2014).
[142]J.-M. Liu, Z. G. Liu, H. L. W. Chan, and C. L. Choy, Mater. Lett. **57**, 1520 (2003).
[143]L.-F. Wang and J.-M. Liu, J. Appl. Phys. **98**, 064106 (2005).
[144]J.-M. Liu, H. Yu, B. Pan, and X. Y. Chen, Mater. Sci. Eng. B **118**, 2 (2005).
[145]H. B. Zuo, M. F. Zhang, J. C. Han, and J.-M. Liu, Mater. Lett. **61**, 2697 (2007).
[146]J.-M. Liu, H. L. W. Chan, C. L. Choy, and C. K. Ong, Phys. Rev. B **65**, 014416 (2001).
[147]D. Guyomar, B. Ducharne, and G. Sébald, J. Phys. D: Appl. Phys. **40**, 6048 (2007).
[148]D. Guyomar, B. Ducharne, and G. Sebald, J. Appl. Phys. **107**, 114108 (2010).
[149]L. Baudry, I. A. Luk'yanchuk, and A. Razumnaya, Ferroelectrics **461**, 22 (2014).
[150]L. Baudry, I. A. Luk'yanchuk, and A. Razumnaya, Phys. Rev. B **91**, 144110 (2015).
[151]M. Iwata and Y. Ishibashi, Jpn. J. Appl. Phys. **38**, 5670 (1999).
[152]Y. Ishibashi and M. Iwata, Jpn. J. Appl. Phys. **38**, 800 (1999).
[153]M. H. Lente and J. A. Eiras, J. Appl. Phys. **92**, 2112 (2002).
[154]A. Tagantsev, L. E. Cross, and J. Fousek, *Domains in Ferroic Crystals and Thin Films* (Springer-Verlag, New York, 2010), p. 470.
[155]H. Tutu and N. Fujiwara, J. Phys. Soc. Jpn. **73**, 2680 (2004).
[156]T. Yasui, H. Tutu, M. Yamamoto, and H. Fujisaka, Phys. Rev. E **66**, 036123 (2002).
[157]B. K. Chakrabarti and M. Acharyya, Rev. Mod. Phys. **71**, 847 (1999).
[158]D. A. Scrymgeour, V. Gopalan, A. Itagi, A. Saxena, and P. J. Swart, Phys. Rev. B **71**, 184110 (2005).
[159]A. J. Bell, J. Appl. Phys. **89**, 3907 (2001).
[160]Y. L. Li, L. E. Cross, and L. Q. Chen, J. Appl. Phys. **98**, 064101 (2005).
[161]J. Hlinka and P. Márton, Phys. Rev. B **74**, 104104 (2006).
[162]J. Íñiguez, S. Ivantchev, J. M. Perez-Mato, and A. García, Phys. Rev. B **63**, 144103 (2001).
[163]A. Kumar and U. V. Waghmare, Phys. Rev. B **82**, 054117 (2010).
[164]J. Mangeri, K. C. Pitike, S. P. Alpay, and S. Nakhmanson, npj Comput. Mater. **2**, 16020 (2016).
[165]Z. Jiang, R. Zhang, F. Li, L. Jin, N. Zhang, D. Wang, and C.-L. Jia, AIP Adv. **6**, 065122 (2016).
[166]B. Wang, *Mechanics of Advanced Functional Materials* (Springer-Verlag, Berlin, Heidelberg, 2013), pp. 345–346.
[167]P. Marton, A. Klíč, M. Paściak, and J. Hlinka, e-print arXiv:1705.08235.

[168]C.-L. Jia, V. Nagarajan, J.-Q. He, L. Houben, T. Zhao, R. Ramesh, K. Urban, and R. Waser, Nat. Mater. **6**, 64 (2007).
[169]J. Hlinka, Ferroelectrics **349**, 49 (2007).
[170]Q. Meng, M.-G. Han, J. Tao, G. Xu, D. O. Welch, and Y. Zhu, Phys. Rev. B **91**, 054104 (2015).
[171]A. Tagantsev, L. E. Cross, and J. Fousek, *Domains in Ferroic Crystals and Thin Films* (Springer-Verlag, New York, 2010), pp. 339–340.
[172]M. H. Lente and J. A. Eiras, J. Phys. Condens. Matter **12**, 5939 (2000).
[173]V. Fridkin and S. Ducharme, *Ferroelectricity at the Nanoscale: Basics and Applications* (Springer-Verlag, Berlin, Heidelberg, 2014), p. 24.
[174]V. L. Ginzburg, Zh. Eksp. Teor. Fiz. **19**, 36 (1949).
[175]V. L. Ginzburg, Phys. Usp. **38**, 490 (1949).
[176]N. C. Cassol-Seewald, M. I. M. Copetti, and G. Krein, Comput. Phys. Commun. **179**, 297 (2008).
[177]J. F. Scott, D. Galt, J. C. Price, J. A. Beall, R. H. Ono, C. A. Paz de Araujo, and L. D. McMillan, Integr. Ferroelectr. **6**, 189 (1995).
[178]C. Elissalde and J. Ravez, J. Mater. Chem. **11**, 1957 (2001).
[179]M. J. Highland, T. T. Fister, M.-I. Richard, D. D. Fong, P. H. Fuoss, C. Thompson, J. A. Eastman, S. K. Streiffer, and G. B. Stephenson, Phys. Rev. Lett. **105**, 167601 (2010).
[180]S. Ducharme, V. Fridkin, R. Gaynutdinov, M. Minnekaev, A. Tolstikhina, and A. Zenkevich, e-print arXiv:1204.4792.
[181]V. Fridkin, A. Ievlev, K. Verkhovskaya, G. Vizdrik, S. Yudin, and S. Ducharme, Ferroelectrics **314**, 37 (2005).
[182]R. Gaynutdinov, S. Yudin, S. Ducharme, and V. Fridkin, Ferroelectrics **429**, 7 (2012).
[183]R. Gaynutdinov, S. Yudin, S. Ducharme, and V. Fridkin, J. Phys. Condens. Matter **24**, 015902 (2012).
[184]S. Ducharme, V. M. Fridkin, A. V. Bune, S. P. Palto, L. M. Blinov, N. N. Petukhova, and S. G. Yudin, Phys. Rev. Lett. **84**, 175 (2000).
[185]J. Y. Jo, D. J. Kim, Y. S. Kim, S.-B. Choe, T. K. Song, J.-G. Yoon, and T. W. Noh, Phys. Rev. Lett. **97**, 247602 (2006).
[186]G. Vizdrik, S. Ducharme, V. M. Fridkin, and S. G. Yudin, Phys. Rev. B **68**, 094113 (2003).
[187]A. Tagantsev, L. E. Cross, and J. Fousek, *Domains in Ferroic Crystals and Thin Films* (Springer-Verlag, New York, 2010).
[188]S. Liu, I. Grinberg, and A. M. Rappe, Nature **534**, 360 (2016).
[189]J. Paul, T. Nishimatsu, Y. Kawazoe, and U. V. Waghmare, Phys. Rev. B **80**, 024107 (2009).
[190]L. Baudry, J. Appl. Phys. **86**, 1096 (1999).